
Article:
Le, HD, Loveday, SM, Singh, H et al. (1 more author) (2020) Gastrointestinal digestion of Pickering emulsions stabilised by hydrophobically modified cellulose nanocrystals: Release of short-chain fatty acids. Food Chemistry, 320. 126650. ISSN 0308-8146

https://doi.org/10.1016/j.foodchem.2020.126650

Highlights

- Pickering emulsions (PEs) were stabilised by modified cellulose nanocrystals
- PEs were used as novel delivery vehicles (DVs) for short-chain fatty acids (SCFAs)
- PEs demonstrated droplet flocculation but no coalescence during gastric digestion
- Gastric flocculation reduced droplet surface area and altered the lipolysis profile
- SCFAs (~ 65%) remaining in the intestinal digesta suggest PEs as effective DVs

Gastrointestinal digestion of Pickering emulsions stabilised by hydrophobically modified cellulose nanocrystals: release of short-chain fatty acids

Hoang Du Le[a,b], Simon M. Loveday[b,c], Harjinder Singh[b], Anwesha Sarkar[a,*]

[a] *Food Colloids and Bioprocessing Group, School of Food Science and Nutrition, University of Leeds, Leeds LS2 9JT, UK*

[b] *Riddet Institute, Massey University, Private Bag 11 222, Palmerston North 4442, New Zealand*

[c] *Food and Bio-based Products Group, AgResearch Ltd, Private Bag 11 008, Palmerston North 4442, New Zealand*

***Corresponding author:**

E-mail address: A.Sarkar@leeds.ac.uk (A. Sarkar).

Food Colloids and Bioprocessing Group,

School of Food Science and Nutrition,

University of Leeds, Leeds LS2 9JT, UK.

Abstract

This study aimed to deliver short-chain fatty acids (SCFAs, including propionic and butyric acids) using Pickering emulsions stabilised by hydrophobically modified cellulose nanocrystals (MCNCs). The emulsions (20 wt% oil, 1 wt% MCNCs) were subjected to two in vitro digestion pathways. In the first pathway, the emulsions were used for direct intestinal digestion by bypassing the gastric phase while in the second pathway, the emulsions were subjected to sequential gastrointestinal digestion. Flocculation of emulsion droplets occurred because of charge screening effects by the gastric electrolytes. Such gastric flocculation reduced the droplet surface area, overall lipolysis kinetics and consequently decreased the extent of SCFA release, latter was 40–45% in the gastric-bypassed emulsions and 30–35% in the sequentially-digested emulsions. High proportion of SCFAs remaining after the intestinal digestion (~ 65%) shows promise in the use of Pickering emulsions for the colon-targeted delivery of SCFAs.

Chemical Compounds Studied in this Article

Tripropionin (PubChem CID: 8763); Tributyrin (PubChem CID: 6050); Propionic acid (PubChem CID: 1032); Butyric acid (PubChem CID: 264).

Keywords: Pickering emulsions; Cellulose nanocrystals; Hydrophobic modification; Lipid digestion; Short-chain fatty acids

50 ## 1. Introduction

51 Short-chain fatty acids (SCFAs) are important functional metabolites. There is
52 clinical evidence to show that they are useful in the prevention of the metabolic
53 syndrome, bowel disorders and certain types of cancer (Besten, Eunen, Groen,
54 Venema, Reijngoud, & Bakker, 2013; Tan, McKenzie, Potamitis, Thorburn, Mackay,
55 & Macia, 2014; Venegas et al., 2019). SCFAs, which are fermentation products of
56 non-digestible carbohydrates by the gut microbiota, consist of six or fewer carbon
57 molecules; the main products of the fermentation are acetic, propionic and butyric
58 acids (95% of the total SCFAs) (Besten et al., 2013). Although SCFAs are produced
59 by the gut bacteria, the total amount and their relative proportions vary depending on
60 the sources of the carbohydrates in the diet (Boets et al., 2015; Knudsen,
61 Jørgensen, & Theil, 2016; Tan et al., 2014; Wang et al., 2017). Therefore, controlling
62 the types and the total amount of SCFAs in the colon might be a good nutritional
63 strategy to achieve therapeutic benefits; this can be accomplished by the use of
64 targeted SCFA precursors, e.g. tripropionin (glyceryl tripropionate, TP) and tributyrin
65 (glyceryl tributyrate, TB) as sources of propionic acid and butyric acid respectively.
66 Oral supplementation of such short-chain triglycerides is an alternative
67 administration route to provide SCFAs directly for those who do not consume
68 sufficient fibre and/or whose gut microbiota is low on SCFA-producing microbes.

69 To date, conventional oil-in-water (O/W) emulsions are the most common
70 systems for the delivery of SCFAs to the colon (Donovan, Bauer, Jr, & Lee, 2017;
71 Donovan, Cadwallader, & Lee, 2016a; Donovan, Lee, & Lee, 2016b; Le, M.Loveday,
72 Nowak, Niu, & Singh, 2020; Li, Maux, Xiao, & McClements, 2009). Although various
73 surfactants or biopolymers (inulin, gamma-cyclodextrin, soy protein isolate and whey
74 protein isolate) or a combination thereof have been used, in most cases only a

75 limited proportion of the SCFAs is eventually delivered to the colon. For instance,
76 reconstituted emulsions from spray-dried TB-loaded powder showed a release of
77 approximately 94% butyric acid in the in vitro small intestinal phase before the
78 colonic regime (Donovan et al., 2017). This was attributed to the enzymatic
79 hydrolysis of the TB in the small intestinal phase (Donovan et al., 2017).
80 Furthermore, most protein-stabilised emulsions tend to be destabilised in the gastric
81 phase because of pepsin-induced interfacial proteolysis results in generation
82 peptides and remnants of proteins at the interface that are not viscoelastic enough to
83 protect the droplets against coalescence (Sarkar, Goh, Singh, & Singh, 2009;
84 Sarkar, Zhang, Murray, Russell, & Boxall, 2017; Torres, Murray, & Sarkar, 2019).
85 More importantly, the competitive displacement of these peptides and remnants of
86 proteins by intestinal bile salts allow the adsorption of lipase on to the bile-coated
87 droplet surface and consequently accelerate the kinetics of lipid digestion (Sarkar,
88 Ye, & Singh, 2016b; Wilde & Chu, 2011). Therefore, to deliver SCFAs to the colon,
89 the interfacial materials must possess two essential properties: (1) resistance to
90 enzymatic degradation during the gastrointestinal transit; (2 resistance to bile salt-
91 mediated competitive displacement. Cellulosic particles are potential candidates that
92 are not degraded by human gastrointestinal enzymes (Sarkar, Zhang, Holmes, &
93 Ettelaie, 2019). In addition, after suitable modification, such cellulosic particles are
94 known to adsorb to the oil–water interface almost irreversibly via a Pickering
95 stabilisation mechanism thus preventing bile salt-mediated displacement (Le,
96 Loveday, Singh, & Sarkar, 2020).

97 Pickering emulsions are stabilised by solid particles that have a strong
98 resistance to bile salt displacement by virtue of their high desorption energy once
99 adsorbed (Sarkar, Murray, Holmes, Ettelaie, Abdalla, & Yang, 2016a; Tzoumaki,

100 Moschakis, Kiosseoglou, & Biliaderis, 2011). Needle-shaped cellulose nanocrystals
101 (CNCs) are human-enzyme-resistant particles that have recently attracted research
102 attention in the production of such Pickering emulsions (Chen, Zheng, Xu, Yin, Liu, &
103 Tang, 2018; Lee, Quero, Blaker, Hill, Eichhorn, & Bismarck, 2011; Yan et al., 2017).
104 A recent study reported successful use of a particular variety of unmodifed CNCs to
105 produce stable and fine emulsions (Qiu-Hong, ChenaTong-Xun, & Chuan-HeTang,
106 2019). However, in most reported studies, CNCs, particularly the sufated ones that
107 are available commercially, have poor wettability in the oil phase, and the stability of
108 unmodified CNC-stabilised Pickering emulsions is usually low (Le et al., 2020);
109 therefore, further application of these emulsions is limited. To overcome this
110 limitation, hydrophobic modification has been used to improve the wettability of
111 CNCs in the oil phase and thus to enhance the stability of the emulsion. To date,
112 various chemicals have been used to modify CNCs, such as succinic anhydride (Liu,
113 Sun, Zhang, Ren, & Geng, 2006), hexanoic acid and dodecanoic acid (Lee et al.,
114 2011), phenyltrimethylammonium chloride (Gong, Wang, & Chen, 2017) and octenyl
115 succinic anhydride (OSA) (Chen et al., 2018). For food application, OSA is the
116 preferred candidate because it has been used in the food industry to modify starch
117 for decades (Nilsson & Bergenståhl, 2007; da Silva et al., 2013). It suggests that
118 OSA–CNCs could be a potential biocompatible Pickering stabilizer in the future. In
119 addition, amphipathic property obtained after OSA modification significantly
120 improved the wettability of CNCs in the oil phase and the emulsion stability against
121 coalescence was demonstrated for longer storage periods (Le et al., 2020).

122 In our previous study (Le et al., 2020), we successfully modified CNCs using
123 OSA and characterised the physicochemical properties of Pickering emulsions
124 stabilised by these modified CNCs (MCNCs) under various pH and ionic conditions.

125 The aim of this current study was to investigate the gastrointestinal digestion
126 properties of the MCNC-stabilised emulsion, to understand its suitability as a delivery
127 vehicle for SCFAs in the targeted digestive tracts. In addition, we also assessed the
128 microstructural fate of these emulsions during in vitro gastrointestinal digestion as
129 well as the degree and rate of SCFA (i.e. propionic and butyric acids) release from
130 these MCNC-stabilised Pickering emulsions in the intestinal phase. The hypothesis
131 of this study was that particle-stabilised emulsions would protect SCFAs during
132 intestinal digestion and thus allow more colon-targeted release. In addition, exposure
133 to gastric conditions may induce microstructural changes in the Pickering emulsions,
134 which might influence the rate and extent of lipolysis and consequently SCFA
135 release profiles. Therefore, we analysed the in vitro digestion of the emulsions using
136 the two routes i.e. sequential gastric and intestinal digestion and intestinal digestion
137 bypassing the gastric step (i.e. without the gastric digestion step).

138

139 2. Materials and methods

140 *2.1. Materials*

141 Sulphated cellulose nanocrystal (CNC, 94–96%) powder was purchased from
142 CelluForce™, Montreal, Quebec, Canada. The CNCs used in this study were
143 intended for research purposes and not for consumption. Sunflower oil (SO) was
144 purchased from a local supermarket (Morrisons, Leeds, UK). Food-grade tripropionin
145 (glyceryl tripropionate ≥ 97.1%, TP) and tributyrin (glyceryl tributyrate ≥ 97.1%, TB),
146 and analytical grade TP, TB, OSA, propionic acid (PA), butyric acid (BA), caproic
147 acid, porcine pepsin (P7000), porcine bile extract (B8631) and porcine pancreatin
148 (P7545, 8 × USP) were purchased from Sigma–Aldrich Company Ltd, Dorset, UK.

149 The standards TP, TB, PA and BA were later used for gas chromatography (GC)
150 analysis. All other chemicals were of analytical grade and were also purchased from
151 Sigma–Aldrich Company Ltd, Dorset, UK. Milli-Q water (electrical resistance of 18.2
152 MΩ.cm at 25 ^{o}C) purified by a Milli-Q apparatus, Millipore Corp., USA, was used as a
153 solvent for all experiments.
154

155 ***2.2. Hydrophobic modification of CNCs***

156 Hydrophobic modification of CNCs was conducted according to a method
157 described by Le et al. (2020). Briefly, the CNC dispersion (3.0 wt% in water) was
158 mixed with OSA at ratio of 1:0.15 (w/w) with the pH maintained at pH 8.3 ± 0.1 for
159 7.0 h. Subsequently, the resultant product was neutralised to pH 7.0 with 1.0 N HCl
160 and then freeze dried, yielding a white powder. Soxhlet extraction with ethanol was
161 then applied to remove any remaining OSA from the powder. Finally, the powder
162 was air dried in an oven at 40 °C overnight to remove the ethanol. This powder is
163 referred to as MCNCs and was used to produce O/W emulsions. Degree of
164 substitution (DS) of the MCNC that was defined as the number of OSA groups per
165 glucose unit was quantified using a titration method (Morrosa, Leveckeb, & Infantea,
166 2011). In the current study, MCNCs had a DS of 0.189. In addition, detailed
167 characterisation of MCNCs and MCNC-stabilised Pickering O/W emulsions has been
168 provided by Le et al. (2020).
169

170 ***2.3. Preparation of Pickering O/W emulsions***

171 The oil phase (a TP–TB–SO mixture with a weight ratio of 1:1:2) was pre-
172 homogenised with the aqueous phase, at a ratio of 1:4 (w/w) to obtain 20 wt% oil

173 and 1.0 wt% MCNCs in the final emulsions, using a high-speed blender (D500
174 series, Biolab Ltd, Germany) at 10,000 rpm for 3 min. In the next step, the coarse
175 emulsions were homogenised using a two-stage valve homogeniser (Panda Plus,
176 GEA Niro Soavi, Italy) at pressures of 200/50 bar using three passes. The emulsions
177 obtained (pH ≈ 7.0) were analysed for droplet size, ζ-potential and microstructure
178 and were subjected to in vitro gastrointestinal digestion.
179

180 ***2.4. In vitro gastrointestinal digestion***

181 The gastrointestinal digestion was carried out using the static INFOGEST
182 digestion protocol described by Minekus et al. (2014) without the oral phase.
183 For gastric digestion, freshly prepared emulsions were mixed with simulated
184 gastric fluid (SGF) buffer (without or with added pepsin) at a ratio of 1:1 v/v under
185 magnetic stirring at 350 rpm. The composition of the SGF was 0.514 g L^{-1} KCl, 0.123
186 g L^{-1} KH_2PO_4, 2.1 g L^{-1} $NaHCO_3$, 2.758 g L^{-1} NaCl, 0.0203 g L^{-1} $MgCl_2(H_2O)_6$, 0.048
187 g L^{-1} $CaCl_2.2H_2O$ and pepsin (2000 U mL^{-1} in the final mixture). The temperature
188 was maintained at 37 ^oC during the digestion and the initial pH was adjusted to pH
189 3.0. Aliquots were collected during 2 h of incubation in the SGF for analysis of size,
190 charge and microstructural changes. Freshly prepared emulsions were diluted to 10
191 wt% oil and were used as controls.
192 For intestinal digestion, freshly prepared emulsions as well as gastric digesta
193 (with added pepsin) were used, the latter representing sequential digestion. For
194 these experiments, freshly prepared emulsions were diluted to 5 wt% oil and were
195 used as controls. The gastric digesta were mixed with simulated intestinal fluid (SIF)
196 buffer (without or with added bile salts and pancreatin) at a ratio of 1:1 v/v at 37 ^oC
197 under magnetic stirring at 350 rpm. The composition of the SIF was 0.253 g L^{-1} KCl,

198 0.054 g L^{-1} KH_2PO_4, 3.57 g L^{-1} $NaHCO_3$, 1.12 g L^{-1} NaCl, 0.335 g L^{-1} $MgCl_2(H_2O)_6$
199 and 0.44 g L^{-1} $CaCl_2.2H_2O$, with/without 10 mM bile salts and pancreatin (lipase
200 activity of 2000 mL^{-1} in the final mixture). The temperature was maintained at 37 °C
201 during the digestion and the initial pH was adjusted to pH 7.0. Aliquots were
202 collected over 3 h of intestinal digestion for analysis of size, ζ-potential and
203 microstructural changes. For the analysis of SCFAs, TP and TB, aliquots were
204 collected after 2, 4, 6, 10, 15, 20, 30, 60 and 120 min of intestinal digestion. To stop
205 the hydrolysis reaction, samples were immediately blended with a mixture of
206 extraction solvents (hexane–isopropanol) or were rapidly cooled using ice.

207 ***2.5. Kinetics of free fatty acid release***

208 Determination of the release of FFAs during the intestinal digestion was carried
209 out on fresh emulsions as well as sequential gastric-digested emulsions at 37 °C for
210 2 h while maintaining the pH at 7.0 by the continuous addition of 0.05 M NaOH using
211 a pH-stat (TIM856, Radiometer Analytical, Hach Company, Loveland, CO, USA).
212 The percentage of FFAs released was calculated based on the volume of NaOH
213 consumed, with the hypothesis that lipase will hydrolyse two FFAs per triglyceride
214 molecule (Sarkar et al., 2016b).

215 $$\%FFA = 100 \times \left(\frac{V_{NaOH} \times M_{NaOH} \times M_{w\ lipid}}{2 \times W_{lipid}}\right) \quad (1)$$

216 where V_{NaOH} is the volume of NaOH solution consumed to neutralise the FFAs
217 produced (in L), M_{NaOH} is the molarity of the NaOH solution used (in M), $M_{w\ lipid}$ is the
218 average molecular mass of the triglyceride (in g mol^{-1}) and W_{lipid} (g) is the total mass
219 of lipid present in the sample used for titration.

220 The kinetic parameters for the initial FFA release were calculated using Eqs. (2)
221 and (3), which were adopted from Eqs. (10) and (12) respectively in previous work
222 (Sarkar, Zhang, Holmes, & Ettelaie, 2019).

223 $$\Phi_t = \Phi_{max}[1 - \exp(-k_1 t)] \quad (2)$$

224 $$\Phi_t = \Phi_{max}[1 - \exp(\frac{-6kM_w Dnt^2}{\rho_o d_0^2 \Gamma^{max}})] \quad (3)$$

225 where t is the intestinal digestion time (min), Φ_{max} is the maximum total FFA level (%)
226 and k_1 (s^{-1}) is the first-order rate constant of FFA release (%FFA min^{-1}), which can
227 be calculated using the following equation:

228 $$k_1 = \frac{6kM_w}{d_o.\rho_o} \quad (4)$$

229 where k (mol s^{-1} m^{-2}) is the lipid conversion rate per unit area of the droplet surface,
230 occurring at maximum lipase surface coverage, M_w is the molecular weight of lipid,
231 d_o is the initial average diameter of the emulsions (d_{32}) and ρ_o is the density of the
232 lipid. Γ^{max} is the maximum coverage of the surface by the enzyme, D is the diffusion
233 coefficient of the enzyme in the continuous aqueous phase and n donates the molar
234 concentration of the enzyme in the bulk solution.

235 In this study, Eqs. (2) and (3) were used as the mathematical models; they
236 gave the best fits to the experimental data. All statistics were conducted using R
237 version 3.5.1 (2018-07-02) http://www.R-project.org/. Non-linear fitting was
238 performed using the nls() function implementing a residual minimisation. Significance
239 levels of $p < 0.001$ (***) were achieved in the model fits. The regression curves were
240 superposed with the experimental data, with the parameters and the standard errors
241 of the residuals being summarised in Table 1. The lipolysis half time ($t_{1/2}$, min), i.e.
242 the time required to achieve half lipid digestion, was obtained from the fitted model.

243 ***2.6. Characterisation of O/W emulsions and digesta***

244 The emulsion and digesta samples were characterised using droplet size, ζ-
245 potential and rheology measurements, and the microstructure was assessed using
246 confocal laser scanning microscopy (CLSM). The samples were diluted to a droplet
247 concentration of around 0.01% w/v before analysing the ζ-potential. For size
248 measurement, the undiluted emulsions or the digesta samples were added to a
249 dispersion unit Hydro EV to reach an obscuration of around 10%. The stirring speed
250 of the dispersion unit was set at 2000 rpm. The droplet size distribution was
251 determined at room temperature (25 ^{o}C) by a static light scattering technique using a
252 Mastersizer (3000S series, Malvern Instruments Ltd, Malvern, UK). The relative
253 refractive index, i.e. the ratio of oil (1.456) to the dispersion medium (1.33), was
254 1.095. Mean droplet sizes were reported as Sauter-average diameters (d_{32}) and
255 volume-average diameters (d_{43}) from the size distribution results. Each individual d_{32}
256 and d_{43} value was reported as the mean and standard deviation of at least three
257 reported readings made on triplicate samples.
258 The ζ-potential of the MCNC-stabilised emulsion droplets was measured using
259 a Zetasizer (ZS Nano, Malvern Instruments Ltd, Malvern, UK). The diluted samples
260 (freshly prepared emulsions and digesta) were transferred into DTS1070 folded
261 capillary cells, followed by 2 min of equilibration within the equipment to reach a
262 temperature of 37 ^{o}C. The machine was controlled by Zetasizer 3000 software that
263 recorded mobilities; the mobility values were then converted to ζ-potential values
264 using the classical Smoluchowski equation. Each ζ-potential value was reported as
265 the mean and standard deviation of at least three reported readings made on
266 triplicate samples.
267 A Kinexus ultra rheometer (Malvern Instruments Ltd, Malvern, UK) was used to
268 measure the apparent viscosity, elastic modulus (G') and viscous modulus (G'') of

269 the emulsions and the digesta. The samples were added to a double gap geometry
270 DG 24/27, followed by 5 min of equilibration to reach a temperature of 37 °C.
271 Subsequently, steady shear experiments were performed; apparent viscosities, as a
272 function of shear rate in the range from 0.1 to 1000 s^{-1}, were recorded. A strain
273 amplitude sweep from 0.1 to 20% was performed for each sample in an attempt to
274 linear viscoelastic region (LVR). Dynamic frequency sweep tests were then carried
275 out at a strain amplitude selected from the strain amplitude sweep (1.0%) and with
276 an angular frequency range of 0.01–20 s^{-1}. The frequency-dependent curves of G'
277 and G'' were recorded. All measurements were done in triplicate and were reported
278 as the mean and standard deviation.

279 CLSM images of the emulsions and the digesta were taken using a Zeiss LSM
280 880 confocal microscope (Carl Zeiss MicroImaging GmbH, Jena, Germany). Exactly
281 500 μL of emulsion was mixed with 10 μL of Nile red (0.1% w/v in dimethyl
282 sulphoxide, excitation 514 nm), 20 μL of Fast green (1.0% w/v in Milli-Q water,
283 excitation 633 nm) and 100 μL of Calcofluor white (1.0% w/v in Milli-Q water,
284 excitation 405 nm). The mixture was vortexed for 10 s and equilibrated for 10 min;
285 then 30 μL was placed on to a concave slide. The sample was covered with a
286 coverslip and was observed using a 40 × magnification oil immersion objective lens.

287 ***2.7. Quantification of TP and TB***

288 Determination of TP and TB was done following a modified GC method as
289 described by Donovan et al. (2016a).

290 *2.7.1. Sample preparation*

291 TP and TB were extracted by mixing 100 μL of sample (emulsion or digesta) with
292 900 μL of a hexane–isopropanol mixture (3:2 w/w ratio). The mixture was vortexed

293 for 20 s and subsequently centrifuged at 17,000 *g* and 2 °C for 20 min. The
294 supernatant (200 µL) was blended with 1800 µL of the hexane–isopropanol mixture
295 and then centrifuged at 17,000 *g* and 2 °C for 20 min. Subsequently, the supernatant
296 was taken for GC analysis. Standard curves were prepared from TP and TB
297 standards at various concentrations using the same protocol.

298 *2.7.2. Chromatographic analysis*

299 TP and TB were analysed using an Agilent 7890A GC system equipped with a
300 flame ionisation detector, a liquid injector, a 7683B autosampler and an Agilent
301 19091Z–413 HP–1 capillary column (30 m x 0.32 mm x 0.25 µm). The carrier gas
302 was helium at a pressure of 7.5 psi, a flow rate of 0.65 mL min^{-1} and velocity µ =
303 22.3 cm s^{-1}. The injection port was set at 300 °C. The oven temperature programme
304 was as follows: 125 °C for 5 min, an increase at 10 °C min^{-1} to 325 °C and held at
305 325 °C for 20 min. The concentrations of TP and TB were calculated based on the
306 peak areas associated with TP and TB, and the standard curves.

307

308 ***2.8. Quantification of PA and BA***

309 PA and BA were measured using a GC method following the adjusted protocol of
310 Bindelle, Pieper, Montoya and Kessel (2011).

311 *2.8.1. Sample preparation*

312 For each sample, 1.0 mL of sample (emulsion or digesta) was first centrifuged
313 at 17,000 *g* and 2 °C for 20 min. The supernatant (200 µL) was mixed with 800 µL of
314 acetonitrile, 60 µL of phosphoric acid (25% w/w) and 400 µL of internal standard
315 (caproic acid, 2 mg mL^{-1} in Milli-Q water). The mixture was centrifuged at 17,000 *g*
316 and 2 °C for 20 min. The supernatant was transferred into a vial to be analysed by

317 GC. Standard curves were prepared from PA and BA standards at various
318 concentrations using the same procedure.

319 *2.8.2. Chromatographic analysis*

320 PA and BA were analysed using a Shimadzu–2010 GC system equipped with a
321 flame ionisation detector, a liquid injector and a Shimadzu–AOC–5000 autosampler.
322 Samples were run on a fused-silica capillary column (30 m x 0.32 mm x 0.25 μm,
323 ZB–FFAP, Zebron). The flow rate of helium (as a carrier gas) was 1.24 mL min^{-1}.
324 The split mode was run with a split ratio of 20:1 at a pressure of 54.4 kPa and a total
325 flow of 29 mL min^{-1}. The temperature programme was as follows: an initial
326 temperature of 100 ^{o}C for 4 min, 170 ^{o}C for 5 min and a final temperature of 220 ^{o}C
327 for 2 min. The concentrations of PA and BA were calculated based on the peak
328 areas associated with PA and BA, and the standard curves.

329 ***2.9. Statistical analysis***

330 Analysis of variance was conducted using Minitab® version 17.3.1 to detect
331 overall significant differences ($p < 0.05$).

332

333 **3. Results and discussion**

334 ***3.1. Microstructural fate of the emulsions – gastric digestion***

335 Pickering emulsions stabilised by 1.0 wt% MCNCs had average diameters d_{32}
336 and d_{43} of 0.06 μm and 0.62 μm respectively (Fig. 1). The freshly prepared
337 emulsions had a bimodal distribution, with the first peak ranging from around 0.01 to
338 0.30 μm and with the second peak being distributed in the narrow droplet size range
339 of 0.30–6.31 μm. The first peak was associated with unadsorbed MCNCs in the
340 aqueous phase, in line with previous work (Le et al., 2020). The emulsions had a

341 homogeneous distribution of droplets, as shown in the CLSM images, with most
342 droplets being well separated and covered by a thin layer of MCNCs (Fig. 1A). In
343 addition, the emulsions were negatively charged at both pH 7.0 and the gastric pH of
344 3.0 (–68.7 mV and –30.1 mV respectively) (Fig. 2), in line with a previous report
345 (Sarkar et al., 2017). The highly negative charges ensured sufficient electrostatic
346 repulsion between the emulsion droplets to prevent aggregation, as shown in the
347 CLSM image in Fig. 1A. On exposure to SGF buffer, the droplet size increased by
348 approximately eight times ($p < 0.05$), with the second peak showing broadening and
349 with the simultaneous appearance of a third peak at around 100 μm; the first peak
350 remained in the same size range but with a lower volumetric proportion (Fig. 1B).
351 The confocal images of the emulsion–SGF buffer mixture in Fig. 1B clearly
352 demonstrate flocculation of the oil droplets. Such an increase in droplet size
353 suggests flocculation and the reduction in the volumetric proportion of the first peak
354 demonstrates the involvement of the unadsorbed MCNCs in the droplet aggregates
355 as shown in our previous study (Le et al., 2020) or involvement of MCNCs to create
356 smaller droplets (Qiu-Hong Chen, Tong-Xun Liu, & Chuan-He Tang, 2019). Our
357 observation was in line with the results of many previous studies that have reported
358 the aggregation of oil droplets stabilised by modified or unmodified CNCs at low pH
359 (Le et al., 2020; Liu et al., 2018; Mikulcov, Bordes, Minarik, & Kasparkov, 2018) and
360 the formation of a gel-like structure at high ionic strengths (Chau et al., 2015; Le et
361 al., 2020; Prathapan, Thapa, Garnier, & Tabor, 2016). In the current study, the
362 simultaneous effects of pH 3.0 and the ionic strength of the gastric conditions led to
363 a significant screening of charges and a reduction in the ζ-potential to –14 mV,
364 compared with –30.1 and –68.7 mV for the freshly prepared emulsion at pH 3.0 and
365 pH 7.0 respectively (Fig. 2). Consequently, the repulsive forces between the droplets

366 were not sufficient to prevent droplet aggregation. However, coalescence was not
367 observed in the emulsion–SGF buffer mixture.

368 Cellulose is known to be not responsive to human proteolytic enzymes such as
369 pepsin (Sarkar et al., 2019), which was the main reason for using this interfacial
370 material for the delivery of SCFAs in this study. As expected, the addition of pepsin
371 did not alter the droplet size of the emulsions significantly ($p < 0.05$) and the overall
372 microstructure showed no coalescence (Fig. 1C), similar to that of the emulsion–
373 SGF buffer (Fig. 1B). In preliminary work (data not shown), 20 wt% O/W emulsions
374 stabilised by pepsin (1.0 wt%) had ζ-potential value of –3.3 mV at pH 3.0. Thus,
375 pepsin would be electrostatically repelled from the anionic MCNC-stabilised
376 emulsions. The ζ-potential data also showed no obvious change on the addition of
377 pepsin ($p > 0.05$) compared with the emulsion–SGF buffer (Fig. 2). In addition, the
378 confocal images in Fig. 1C showed similar droplet aggregation to that in Fig. 1B,
379 confirming the limited contribution of pepsin to the gastric flocculation of MCNC-
380 stabilised emulsions, which is in contrast to most protein-stabilised emulsions, which
381 are highly susceptible to interfacial proteolysis (Sarkar et al., 2009, 2017; Torres et
382 al., 2019).

383 The effects of SGF buffer, without and with the addition of pepsin, on the
384 rheological properties (apparent viscosity, elastic modulus and viscous modulus) of
385 the emulsions were determined (Supplementary Fig. S1). Freshly prepared
386 emulsions with 10 wt% oil had a low viscosity and Newtonian behaviour. The
387 presence of SGF buffer with or without pepsin led to significant changes in the
388 rheological properties of the emulsion. For example, at a shear rate of 10 s^{-1}, the
389 viscosity increased by approximately 27 times (Fig. S1A), which was due to floc
390 formation under the SGF conditions, in line with a previous study (Le et al., 2020). In

391 addition, the elastic and viscous moduli presented in Fig. S1B clearly demonstrate
392 the formation of a gel-like structure; the elastic modulus was approximately 10 times
393 higher than the viscous modulus and there was little frequency dependence of the
394 two moduli (Ikeda & Nishinari, 2001). In summary, it can be suggested that the
395 electrostatic charge screening of the emulsion droplets was the main mechanism
396 behind the flocculation under gastric conditions.

397 ***3.2. Microstructural fate of the emulsions – intestinal digestion***

398 *3.2.1. Bypassing gastric digestion*

399 The purpose of this intestinal digestion was to understand the ability of
400 Pickering emulsions on their own to protect SCFAs in the intestine. Therefore,
401 freshly prepared emulsions were diluted twice (10 wt% oil) and subsequently used
402 for intestinal digestion without going through the gastric stage. Three different
403 systems were used for this intestinal digestion: emulsion–SIF buffer; emulsion–SIF
404 buffer containing bile salts; emulsion–SIF buffer containing bile salts and pancreatin.
405 Fig. 3A shows that the addition of SIF buffer slightly increased the average size (d_{43})
406 of the emulsion droplets (Fig. 1A). The confocal image demonstrated some degree
407 of droplet flocculation but the majority of the droplets were still well separated. In
408 addition, the ζ-potential of the emulsions decreased significantly from –68.7 mV
409 (freshly prepared emulsion) to –47.8 mV in the emulsion–SIF mixture. The
410 aggregation of the emulsion droplets was due to the reduction in the electrostatic
411 repulsion in the presence of electrolytes. Similar observations have been reported in
412 previous studies (Chau et al., 2015; Le et al., 2020; Prathapan et al., 2016). In
413 addition, SIF contains divalent cations (Ca^{2+} ions), which might induce ion bridging
414 between MCNCs adsorbed on to different droplets. Such ion binding could have

415 resulted in a more viscous shear-thinning structure compared with the freshly
416 prepared emulsions (Supplementary Figs. S1 and S2).

417 The addition of bile salts had limited effect on the ζ-potential and the overall
418 microscopic structure remained unchanged. In addition, the apparent viscosity did
419 not change in the presence of bile salts (Fig. S2). The confocal image in Fig. 3B
420 clearly shows that, in the presence of bile salts, most oil droplets were still
421 encapsulated within the MCNC-stabilised shell and that small aggregates of several
422 oil droplets that had formed through treatment with the buffer remained. This
423 suggests that the displacement by bile salts of MCNCs adsorbed on to the droplet
424 surface was rather restricted. Two main factors may have contributed to the
425 resistance of the MCNCs to bile salt displacement. The first and most important
426 factor was the high desorption energy of the MCNC-laden interface (Sarkar et al.,
427 2016a; Wu & Ma, 2016; Zoppe, Venditti, & Rojas, 2012). It is noteworthy that
428 MCNCs with $r \approx 20$ nm (the width is taken as the radius given that the MCNCs lie flat
429 at the interface) (Le et al., 2020) at a contact angle of 86° at the oil–water interface
430 (typical value of $\gamma_{ow} \approx 50$ mN m^{-1}) will have a desorption energy (ΔE) of nearly $10^5 k_B T$,
431 where k_B is the Boltzmann constant and T is the temperature in Kelvin. Thus, it is
432 unlikely that bile salts can overcome such high energies and thus they cannot
433 displace MCNCs from the interface. Surface charge could be the second factor for
434 the emulsion stability in the presence of bile salts. Under SIF conditions (pH 7.0),
435 both the MCNCs and the bile salts had negative charges. It has been reported that a
436 20 wt% O/W emulsion stabilised by bile salts (1.0 wt%) had a ζ-potential of around –
437 46 mV at pH 7.0 (Sarkar et al., 2016b). However, MCNCs contain hydroxyl, sulphate
438 and OSA groups in their backbones, which make them negatively charged at pH 7.0.
439 Thus, it is highly likely that MCNCs will repel anionic bile salts from the vicinity of

440 negatively charged emulsion droplets. A similar observation was reported in a
441 previous study (Sarkar, Li, Cray, & Boxall, 2018), in which the authors investigated
442 the duodenal digestion of O/W emulsions stabilised by protein coated with
443 unmodified CNCs as primary and secondary layers respectively.

444 The addition of pancreatin significantly increased the droplet size (d_{43}) of the
445 emulsions, changing the distribution from bimodal to trimodal (Fig. 3C). After 5 min of
446 incubation in SIF containing bile salts and pancreatin, the d_{43} of the emulsions
447 increased 50-fold from 0.62 μm (freshly prepared emulsion) or 0.55 μm (emulsion +
448 SIF containing bile salts) to 31.8 μm ($p < 0.05$), whereas the apparent viscosity of the
449 digesta remained unchanged (Supplementary Fig. S3). The confocal image in Fig.
450 3C shows the presence of some larger coalesced droplets, corroborating the third
451 peak in the size distribution, but the majority of the droplets were still encapsulated
452 by MCNCs or trapped within the droplet aggregates. Therefore, the significant
453 increase in size was probably due to both droplet flocculation and some degree of
454 coalescence. Pancreatin addition also resulted in a significant increase in the ζ-
455 potential to –23.9 mV, compared with –47.2 mV in the systems without pancreatin
456 (Fig. 3B). After 30 min of incubation in SIF containing pancreatin and bile salts, the
457 d_{43} value increased to 75.9 μm (Fig. 3D), i.e. twice the size at 5 min, and the
458 confocal image demonstrated a higher degree of coalescence, suggesting that the
459 lipolysis was not complete within the first 5 min. After 3 h of digestion (Fig. 3E),
460 although there was a high degree of coalescence, a significant proportion of the
461 droplets were still intact inside the aggregates. The increase in the negative ζ-
462 potential (–34.1 mV), compared with that after 5 min (Fig. 3C) ($p < 0.05$), might be
463 attributed to the release of lipid digestion products, such as fatty acids and mono-
464 and/or diglycerides, that accumulated on the droplet surface. Similar observations on

465 the changes in surface charge have been reported in previous studies (Sarkar et al.,
466 2018; Wilde & Chu, 2011). Although the Pickering emulsions were capable of
467 resisting bile salt displacement, they did not prevent lipolysis of the oil droplets. This
468 might be expected as the size of the interfacial pores at the MCNC-coated droplets
469 might be an order of magnitude greater than the 2.5-nm-sized lipase molecules
470 (Sarkar et al., 2016a), allowing easy access of lipase to the lipidic substrate.

471 *3.2.2. With gastric digestion – sequential gastrointestinal digestion*

472 To understand the real in vivo fate of the emulsions, they were first subjected to
473 gastric digestion and then the gastric digesta were used for an intestinal digestion in
474 SIF buffer without and with bile salts, and with both bile salts and pancreatin. Fig. 4A
475 shows that the droplet size became smaller after 3 h of incubation in SIF buffer,
476 compared with the gastric digesta (Fig. 1C). The confocal image also revealed the
477 presence of aggregates, which were smaller than those in the gastric digesta (Fig.
478 1C). A possible explanation for this observation was the change in pH, which allowed
479 the ζ-potential to increase from –10.4 mV in the gastric digesta (pH 3.0) to –19.8 mV
480 in the presence of SIF buffer (pH 7.0). As a result, the repulsive forces between the
481 emulsion droplets increased, allowing better separation of the droplets. However, the
482 ζ-potential of the gastric digseta in SIF was significantly lower ($p < 0.05$) than that in
483 the sample without gastric digestion (–47.8 mV) (Fig. 3A). In other words, gastric
484 digestion affected the surface properties of the emulsions and, even after changing
485 the pH, some of the flocculated droplets did not revert to their original individual
486 droplets. In addition, it should be noted that these gastric digesta in SIF contained
487 electrolytes of both the SGF and the SIF; non-gastric-digested samples contained
488 only SIF ions, explaining the lower ζ-potential in the gastric-digested system.

489 The addition of bile salts did not influence the size, ζ-potential, microscopic
490 structure (Fig. 4B) and apparent viscosity of the gastric digesta (Fig. S3). This
491 observation was in line with the results reported in Section 3.2.1, again confirming
492 the excellent resistance of MCNCs to bile salt displacement. The presence of
493 pancreatin altered the droplet size, surface charge and microscopic structure (Figs.
494 4C–4E) dramatically but did not significantly alter the apparent viscosity (Fig. S3).
495 The effects of pancreatin that were observed in these gastric-digested samples were
496 similar to those observed in the gastric-bypassed samples but with a smaller change
497 in absolute values. Qualitatively, after 30 min of incubation in SIF, the ζ-potential of
498 the gastric digesta remained unchanged ($p > 0.05$) compared with that at 5 min.
499 Although size increased dramatically after 5 min of digestion, increasing the
500 incubation time further did not alter the droplet size significantly ($p > 0.05$). In
501 addition, the confocal images did not show any difference in the degree of
502 coalescence (Figs. 4C–4E).

503 ***3.3. Kinetics of fatty acid release and short-chain triglyceride hydrolysis***

504 To quantitatively observe the kinetics of total FFA (including long- and short-
505 chain fatty acids) release in the intestinal phase, titration was employed, followed by
506 fitting with a theoretical model; the release of individual SCFAs, including PA and
507 BA, was quantified by GC. In addition, the degree of lipolysis was determined
508 through quantification of short-chain triglycerides, i.e. TP and TB. An example GC
509 profile of a sequential gastrointestinal-digested sample after 10 min of digestion is
510 reported in Fig. S4.

511 Fig. 5A shows that the Pickering emulsions prepared using MCNCs without
512 going through the gastric route had a relatively slow rate of initial lipid digestion as
513 compared to other Pickering emulsion systems, such as those stabilized by protein-

514 based particles. For instance, the *k* value (0.046 μmol s^{-1} m^{-2}) was nearly 10-fold
515 lower in this study using MCNCs as Pickering stabilizers that observed in case of
516 proteinaceous-microgel particle-stabilized Pickering emulsions (0.31 μmol s^{-1} m^{-2})
517 (Sarkar et al., 2016a). It should also be noted that this initial rate of lipolysis of 1 wt%
518 MCNC-stabilised emulsions is in line with the values reported in the literature when
519 CNCs (3 wt%) were used as a secondary layer to coat protein-stabilised emulsions
520 (Sarkar et al., 2018). This highlights that CNCs, when modified and presented
521 directly at the interface, provide a better barrier to the diffusion of lipase to the
522 droplet surface than the proteinaceous Pickering stabilisers or protein–CNC
523 composite interfacial layers studied previously. Of more importance is that gastric
524 digestion had a significant effect on the degree and the rate of FFA release (Fig. 5A).
525 In the first 10 min, up to 27.5% FFAs were produced in freshly prepared emulsions
526 whereas the release was around 3-fold lower for the gastric-digested emulsions.
527 From the initial hydrolysis period obtained from the fitted parameters using Eqs. (2)
528 and (3), freshly prepared emulsions that bypassed the gastric route were digested
529 significantly faster than their gastric-digested counterparts (Table 1). Passing
530 through gastric digestion increased the overall hydrolysis half time by around 9 min
531 and decreased the maximum FFA release by 27% (Table 1). The delay of the
532 lipolysis after exposing the emulsion to gastric digestion was due to the formation of
533 aggregates and consequently a reduction in the droplet surface area. Our results are
534 in line with a previous study (Golding et al., 2011), in which the authors also
535 highlighted that the rate of intestinal lipolysis was significantly influenced by changes
536 in the droplet surface area that were induced at the gastric stage. In addition to the
537 reduction in surface area, the MCNC-led flocculation also played an important role in
538 trapping a high proportion of the oil droplets inside the aggregates (Figs. 4C–4E),

539 with extra protection from lipase, helping to delay the digestion. The flocculation in
540 the gastric phase thus reduced the available surface area for lipase to bind to and
541 probably created a barrier to the droplets that were trapped inside the aggregates.
542 Also, we hypothesise that the packing of droplets within the aggregates might have
543 reduced the available interfacial pores in which lipase could diffuse or from which
544 lipolytic products (e.g. FFAs, mono- and/or diglycerides) could diffuse out to the
545 aqueous media for analysis by the pH-stat technique.

546 The results in Fig. 5B show a similar pattern to that in Fig. 5A. It is worth noting
547 that there was a significant difference between the release of FFAs (Fig. 5A) and the
548 release of SCFAs (Fig. 5B). During the intestinal digestion, SCFA release was
549 approximately 5–7% higher than FFA release. The difference was due to various
550 lipolysis rates of the different triglycerides, depending on the fatty acid chain length.
551 In the current study, a mixture of SO, TP and TB was used as the oil phase. SO itself
552 consists of a mixture of long-chain triglycerides whereas TP and TB are short-chain
553 triglycerides. Previous studies have shown that lipase has greater affinity towards
554 short-chain triglycerides than to long-chain triglycerides, which was demonstrated
555 using pancreatic lipases from pigs (Liang, Jiang, Yokoyama, Yang, Cao, & Zhong,
556 2016; Nini, Sarda, Comeau, Boitard, Dubèsc, & Chahinian, 2001), rats and humans
557 (Cohen, Morgan, & Hofmann, 1971). This was due to the water solubilities of
558 triglycerides and lipid digestion products. Short-chain triglycerides are relatively more
559 soluble in water than long-chain triglycerides. As a result, the accessibility of lipase
560 to adsorb and hydrolyse short-chain triglycerides is greater than for long-chain
561 triglycerides. In addition, the SCFAs and short-chain mono- and/or di-glycerides
562 obtained from the hydrolysis of short-chain triglycerides have better water solubility
563 than those hydrolysed from long-chain triglycerides. Hence, the diffusion of these

564 hydrolysis products from short-chain triglycerides to the aqueous phase is faster,
565 leaving more available surface for further lipolysis; thus, the proportion of SCFA
566 release was higher than that of long-chain fatty acids. Therefore, the SCFA release
567 quantified by GC was significantly higher than the total FFAs determined by titration.
568 The release patterns of PA and BA were almost identical, with slightly more release
569 of PA (2–3% higher) than of BA.

570 Even though the patterns of TP and TB hydrolysis (Fig. 5C) were similar to
571 those of the fatty acid release seen in both Fig. 5A and Fig. 5B, the hydrolysis
572 proportions of the two short-chain triglycerides were around 5–8% higher than the
573 release proportions of the corresponding SCFAs. In this study, the proportions of
574 short-chain triglyceride hydrolysis were quantified based on the difference between
575 the amounts of short-chain triglycerides present in the emulsions before and after the
576 intestinal digestion. For SCFAs, the release proportion was quantified with the
577 hypothesis that one triglyceride molecule would produce two molecules of
578 corresponding SCFAs. However, it seems that a small proportion of TP and TB
579 produced only one molecule of SCFAs.

580

581 **4. Conclusions**

582 The study demonstrated that Pickering O/W emulsions stabilised by MCNCs
583 were prone to flocculation in a gastric environment. The formation of aggregates was
584 due to a reduction in the electrostatic repulsive force between the emulsion droplets,
585 which was induced by low pH and high ionic strength. Under intestinal conditions,
586 the lipolysis rates were associated with a reduction in the droplet surface area
587 because of gastric structuring, with the gastric-digested emulsions being digested
588 more slowly than freshly prepared emulsions. In addition, electrostatic repulsion of

589 MCNCs to bile salts and the high desorption energy of the MCNCs particles were
590 responsible for the resistance to bile salt displacement, which occurred in the initial
591 stage of the digestion process. The excellent resistance of the MCNC-stabilised
592 emulsion to lipolysis shows its suitability as a delivery system for SCFAs. The
593 responsiveness of these emulsions to gastrointestinal conditions, as shown in this
594 study, might allow the development of novel foods that can deliver other bioactive
595 compounds to target regions of the digestive tract.
596

597 ## Declaration of Competing Interest

598 The authors declare that they have no known competing financial interests.
599

600 ## Acknowledgements

601 Hoang Du Le acknowledges financial support from the Riddet Institute,
602 Massey University, for a travel fellowship to do this research at the University of
603 Leeds, UK, and a PhD scholarship from the New Zealand Ministry of Foreign Affairs
604 and Trade. Author (AS) wishes to thank Dr. Melvin Holmes for valuable suggestions
605 regarding the kinetics of lipid conversion as well as curve fitting. The Zeiss LSM 880
606 microscope used in this work at the University of Leeds, UK, was funded by the
607 Welcome Trust multi-user equipment award WT104918MA.
608

609 ## Appendix A. Supplementary data

610 Supplementary data related to this article can be found online at ….
611

612 ## References

613 Besten, G. D., Eunen, K. V., Groen, A. K., Venema, K., Reijngoud, D.-J., & Bakker,
614 B. M. (2013). The role of short-chain fatty acids in the interplay between diet,
615 gut microbiota, and host energy metabolism. *Journal of Lipid Research, 54*,
616 2325–2340.
617 Bindelle, J., Pieper, R., Montoya, C. A., & Kessel, A. G. V. (2011). Nonstarch
618 polysaccharide-degrading enzymes alter the microbial community and the
619 fermentation patterns of barley cultivars and wheat products in an in vitro
620 model of the porcine gastrointestinal tract. *FEMS Microbiology Ecology, 76*,
621 553–563.
622 Boets, E., Deroover, L., Houben, E., Vermeulen, K., Gomand, S. V., Delcour, J. A., &
623 Verbeke, K. (2015). Quantification of in vivo colonic short chain fatty acid
624 production from inulin. *Nutrients, 7*, 8916–8929.
625 Chau, M., Sriskandha, S. E., Pichugin, D., Thérien-Aubin, H., Nykypanchuk, D.,
626 Chauve, G., Méthot, M., Bouchard, J., Gang, O., & Kumacheva, E. (2015).
627 Ion-mediated gelation of aqueous suspensions of cellulose nanocrystals.
628 *Biomacromolecules, 16*, 2455–2462.
629 Chen, Q.-H., Zheng, J., Xu, Y.-T., Yin, S.-W., Liu, F., & Tang, C.-H. (2018). Surface
630 modification improves fabrication of pickering high internal phase emulsions
631 stabilized by cellulose nanocrystals. *Food Hydrocolloids, 75*, 125–130.
632 Cohen, M., Morgan, R., & Hofmann, A. (1971). Lipolytic activity of human gastric and
633 duodenal juice against medium and long chain triglycerides.
634 *Gastroenterology, 60*, 1–15.
635 da Silva, F. C., da Fonseca, C. R., de Alencar, S. M., Thomazini, M., de Carvalho
636 Balieiro, J. C., Pittia, P., & Fávaro-Trindade, C. S. (2013). Assessment of
637 production efficiency, physicochemical properties and storage stability of

638 spray-dried propolis, a natural food additive, using gum Arabic and OSA
639 starch-based carrier systems. *Food and Bioproducts Processing, 91*, 28–36.
640 Donovan, J. D., Bauer, L., Jr, G. C. F., & Lee, Y. (2017). In vitro digestion and
641 fermentation of microencapsulated tributyrin for the delivery of butyrate.
642 *Journal of Food Science, 82*, 1491–1499.
643 Donovan, J. D., Cadwallader, K. R., & Lee, Y. (2016a). Volatile retention and
644 morphological properties of microencapsulated tributyrin varied by wall
645 material and drying method. *Journal of Food Science, 81*, E643–E650.
646 Donovan, J. D., Lee, S.-Y., & Lee, Y. (2016b). R-index measure of
647 microencapsulated tributyrin in gamma-cyclodextrin influenced by drying
648 method. *Journal of Food Science, 81*, S2252–S2257.
649 Golding, M., Wooster, T. J., Day, L., Xu, M., Lundin, L., Keogh, J., & Clifton, P.
650 (2011). Impact of gastric structuring on the lipolysis of emulsified lipids. *Soft*
651 *Matter, 7*, 3513–3523.
652 Gong, X., Wang, Y., & Chen, L. (2017). Enhanced emulsifying properties of wood-
653 based cellulose nanocrystals as Pickering emulsion stabilizer. *Carbohydrate*
654 *Polymers, 169*, 295–303.
655 Ikeda, S., & Nishinari, K. (2001). “Weak gel”-type rheological properties of aqueous
656 dispersions of nonaggregated κ-carrageenan helices. *Journal of Agricultural*
657 *and Food Chemistry, 49*, 4436–4441.
658 Knudsen, K. E. B., Jørgensen, H., & Theil, P. K. (2016). Changes in short-chain fatty
659 acid plasma profile incurred by dietary fiber composition. *Journal of Animal*
660 *Science, 94*, 476–479.
661 Le, H. D., M.Loveday, S., Nowak, E., Niu, Z., & Singh, H. (2020). Pectin emulsions
662 for colon-targeted release of propionic acid. *Food Hydrocolloids, 103*, 105623.

663 Le, H. D., Loveday, S. M., Singh, H., & Sarkar, A. (2020). Pickering emulsions
664 stabilised by hydrophobically modified cellulose nanocrystals: responsiveness
665 to pH and ionic strength. *Food Hydrocolloids, 99*, 105344.
666 Lee, K.-Y., Quero, F., Blaker, J. J., Hill, C. A. S., Eichhorn, S. J., & Bismarck, A.
667 (2011). Surface only modification of bacterial cellulose nanofibres with organic
668 acids. *Cellulose, 18*, 595–605.
669 Li, Y., Maux, S. L., Xiao, H., & McClements, D. J. (2009). Emulsion-based delivery
670 systems for tributyrin, a potential colon cancer preventative agent. *Journal of*
671 *Agricultural and Food Chemistry, 57*, 9243–9249.
672 Liang, R., Jiang, Y., Yokoyama, W., Yang, C., Cao, G., & Zhong, F. (2016).
673 Preparation of Pickering emulsions with short, medium and long chain
674 triacylglycerols stabilized by starch nanocrystals and their in vitro digestion
675 properties. *RSC Advances, 6*, 99496–99508.
676 Liu, C., Sun, R., Zhang, A., Ren, J., & Geng, Z. (2006). Structural and thermal
677 characterization of sugarcane bagasse cellulose succinates prepared in ionic
678 liquid. *Polymer Degradation and Stability, 91*, 3040–3047.
679 Liu, H., Zhou, C., Liu, X., Xu, Y., Geng, S., Chen, Y., Wei, C., & Yu, C. (2018).
680 PMMA@SCNC composite microspheres prepared from pickering emulsion
681 template as curcumin delivery carriers. *Journal of Applied Polymer Science,*
682 *135*, 46127 (46121–46129).
683 Mikulcov, V., Bordes, R., Minarik, A., & Kasparkov, V. (2018). Pickering oil-in-water
684 emulsions stabilized by carboxylated cellulose nanocrystals: effect of the pH.
685 *Food Hydrocolloids, 80*, 60–67.
686 Minekus, M., Marie, A., Alvito, P., Ballance, S., Bohn, T., Bourlieu, C., Carrière, F.,
687 Boutrou, R., Corredig, M., Dupont, D., Dufour, C., Egger, L., Golding, M.,

Karakaya, S., Kirkhus, B., Feunteun, S. L., Lesmes, U., Macierzanka, A., Mackie, A. R., Marze, S., Mcclements, D. J., Ménard, O., Recio, I., Santos, C. N., Singh, R. P., Vegarud, G. E., Wickham, M. S. J., Weitschies, W., & Brodkorb, A. (2014). A standardised static in vitro digestion method suitable for food – an international consensus. *Food and Function*, 5, 1113–1124.

Morrosa, J., Leveckeb, B., & Infantea, M. R. (2011). Hydrophobically modified inulin from alkenyl succinic anhydride in aqueous media. *Carbohydrate Polymers, 84*, 1110–1116.

Nilsson, L., & Bergenståhl, B. (2007). Adsorption of hydrophobically modified anionic starch at oppositely charged oil/water interfaces. *Journal of Colloid and Interface Science, 308*, 508–513.

Nini, L., Sarda, L., Comeau, L.-C., Boitard, E., Dubèsc, J.-P., & Chahinian, H. (2001). Lipase-catalysed hydrolysis of short-chain substrates in solution and in emulsion: a kinetic study. *Biochimica et Biophysica Acta (BBA) - Molecular and Cell Biology of Lipids, 1534*, 34–44.

Prathapan, R., Thapa, R., Garnier, G., & Tabor, R. (2016). Modulating the zeta potential of cellulose nanocrystals using salts and surfactants. *Colloids and Surfaces A: Physicochemical and Engineering Aspects, 20*, 11–18.

Qiu-Hong, ChenaTong-Xun, & Chuan-HeTang, L. (2019). Tuning the stability and microstructure of fine Pickering emulsions stabilized by cellulose nanocrystals. *Industrial Crops and Products, 141*, 111733.

Sarkar, A., Goh, K. K. T., Singh, R. P., & Singh, H. (2009). Behaviour of an oil-in-water emulsion stabilized by β-lactoglobulin in an in vitro gastric model. *Food Hydrocolloids, 23*, 1563–1569.

712 Sarkar, A., Li, H., Cray, D., & Boxall, S. (2018). Composite whey protein–cellulose
713 nanocrystals at oil–water interface: towards delaying lipid digestion. *Food*
714 *Hydrocolloids, 77*, 436–444.
715 Sarkar, A., Murray, B., Holmes, M., Ettelaie, R., Abdalla, A., & Yang, X. (2016a). In
716 vitro digestion of Pickering emulsions stabilized by soft whey protein microgel
717 particles: influence of thermal treatment. *Soft Matter, 12*, 3558–3569.
718 Sarkar, A., Ye, A., & Singh, H. (2016b). On the role of bile salts in the digestion of
719 emulsified lipids. *Food Hydrocolloids, 60*, 77–84.
720 Sarkar, A., Zhang, S., Holmes, M., & Ettelaie, R. (2019). Colloidal aspects of
721 digestion of Pickering emulsions: experiments and theoretical models of lipid
722 digestion kinetics. *Advances in Colloid and Interface Science, 263*, 195–211.
723 Sarkar, A., Zhang, S., Murray, B., Russell, J., & Boxall, S. (2017). Modulating in vitro
724 gastric digestion of emulsions using composite whey protein-cellulose
725 nanocrystal interfaces. *Colloids and Surfaces B: Biointerfaces, 158*, 137–146.
726 Tan, J., McKenzie, C., Potamitis, M., Thorburn, A. N., Mackay, C. R., & Macia, L.
727 (2014). The role of short-chain fatty acids in health and disease. *Advances in*
728 *Immunology, 121*, 91–119.
729 Torres, O., Murray, B. S., & Sarkar, A. (2019). Overcoming in vitro gastric
730 destabilisation of emulsion droplets using emulsion microgel particles for
731 targeted intestinal release of fatty acids. *Food Hydrocolloids, 89*, 523–533.
732 Tzoumaki, M., Moschakis, T., Kiosseoglou, V., & Biliaderis, C. (2011). Oil-in-water
733 emulsions stabilized by chitin nanocrystal particles. *Food Hydrocolloids, 25*,
734 1521–1529.
735 Venegas, D. P., Fuente, M. K. D. l., Landskron, G., González, M. J., Quera, R.,
736 Dijkstra, G., Harmsen, H. J. M., Faber, K. N., & Hermoso, M. A. (2019). Short

737 chain fatty acids (SCFAs)-mediated gut epithelial and immune regulation and
738 its relevance for inflammatory bowel diseases. *Frontiers in Immunology, 10*,
739 00277.
740 Wang, L., Hu, L., Yan, S., Jiang, T., Fang, S., Wang, G., Zhao, J., Zhang, H., &
741 Chen, W. (2017). Effects of different oligosaccharides at various dosages on
742 the composition of gut microbiota and short-chain fatty acids in mice with
743 constipation. *Food & Function, 8*, 1966–1978.
744 Wilde, P., & Chu, B.-S. (2011). Interfacial & colloidal aspects of lipid digestion.
745 *Advances in Colloid and Interface Science, 165*, 14–22.
746 Wu, J., & Ma, G. H. (2016). Recent studies of pickering emulsions: particles make
747 the difference. *Small, 26*, 4633–4648.
748 Yan, H., Chen, X., Song, H., Li, J., Feng, Y., Shi, Z., Wang, X., & Lin, Q. (2017).
749 Synthesis of bacterial cellulose and bacterial cellulose nanocrystals for their
750 applications in the stabilization of olive oil pickering emulsion. *Food*
751 *Hydrocolloids, 72*, 127–135.
752 Zoppe, J., Venditti, R., & Rojas, O. (2012). Pickering emulsions stabilized by
753 cellulose nanocrystals grafted with thermo-responsive polymer brushes.
754 *Journal of Colloid and Interface Science, 369*, 202–209.

Tables

Table 1

Kinetic parameters of the intestinal digestion during in vitro gastrointestinal digestion.

	k (μmol s^{-1} m^{-2})*	Φ_{max} (%)	$t_{1/2}$ (min)
With gastric digestion	0.001752 (0.00006090)	20.8 (0.09842)	10.98
Without gastric digestion	0.04608 (0.001039)	28.6 (0.07093)	1.93

*Data in parentheses represent the standard errors of the estimates.

k, lipid conversion rate per unit area of the droplet surface.

Φ_{max}, maximum total FFA level.

$t_{½}$, lipolysis half time.

Figures

Figure 1

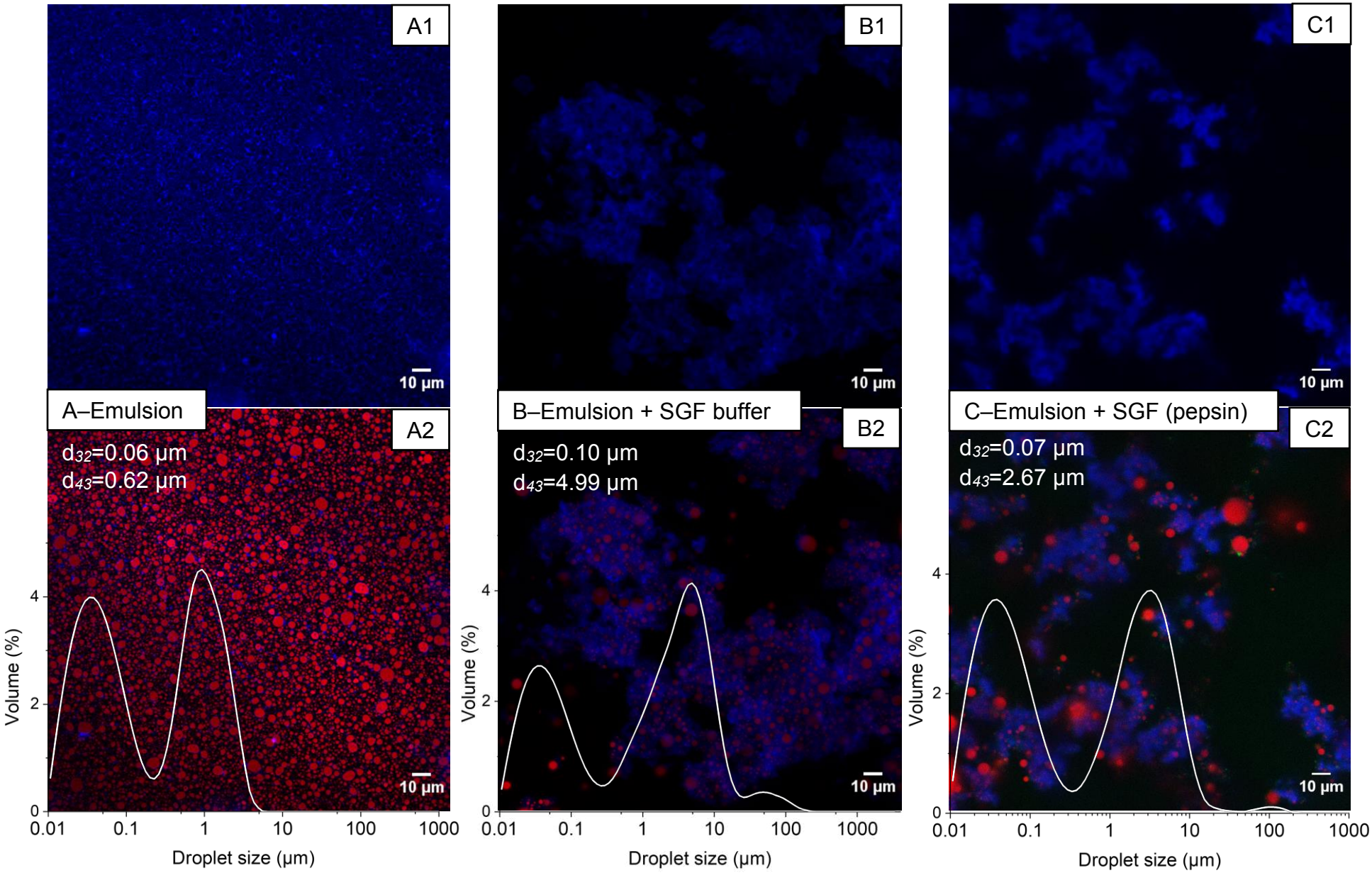

Figure 2

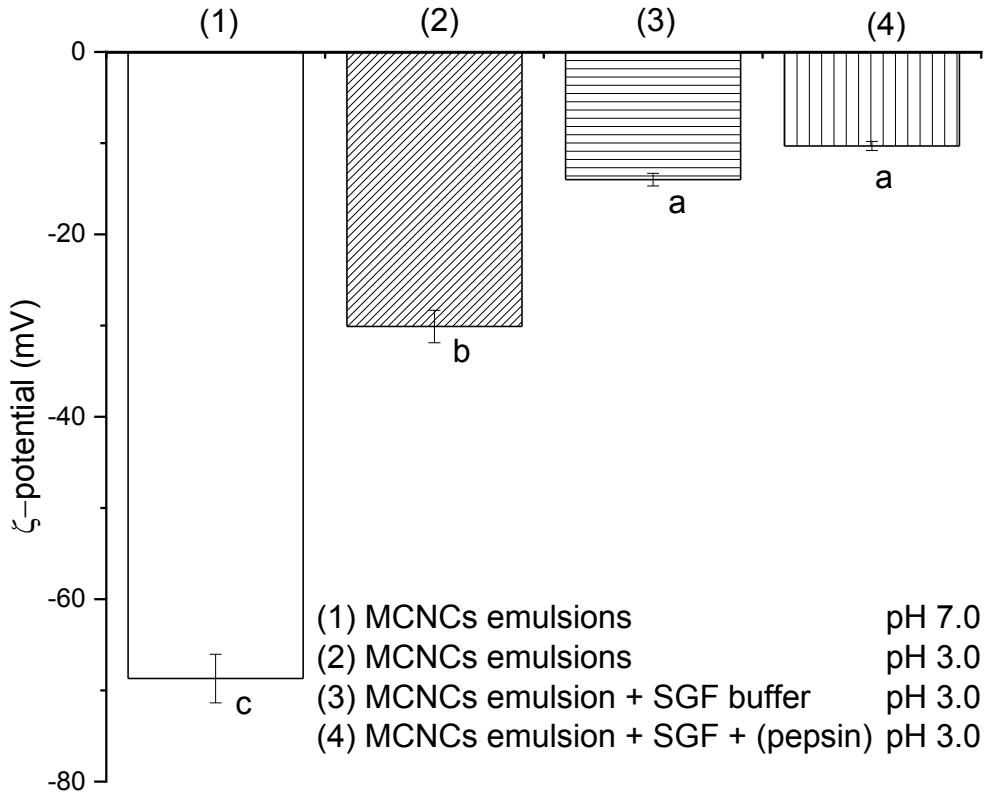
(1)
(2)
(3)
(4)
0
-20
-40
-60
-80
ζ–potential (mV)
a
a
b
c
(1) MCNCs emulsions pH 7.0
(2) MCNCs emulsions pH 3.0
(3) MCNCs emulsion + SGF buffer pH 3.0
(4) MCNCs emulsion + SGF + (pepsin) pH 3.0

Figure 3

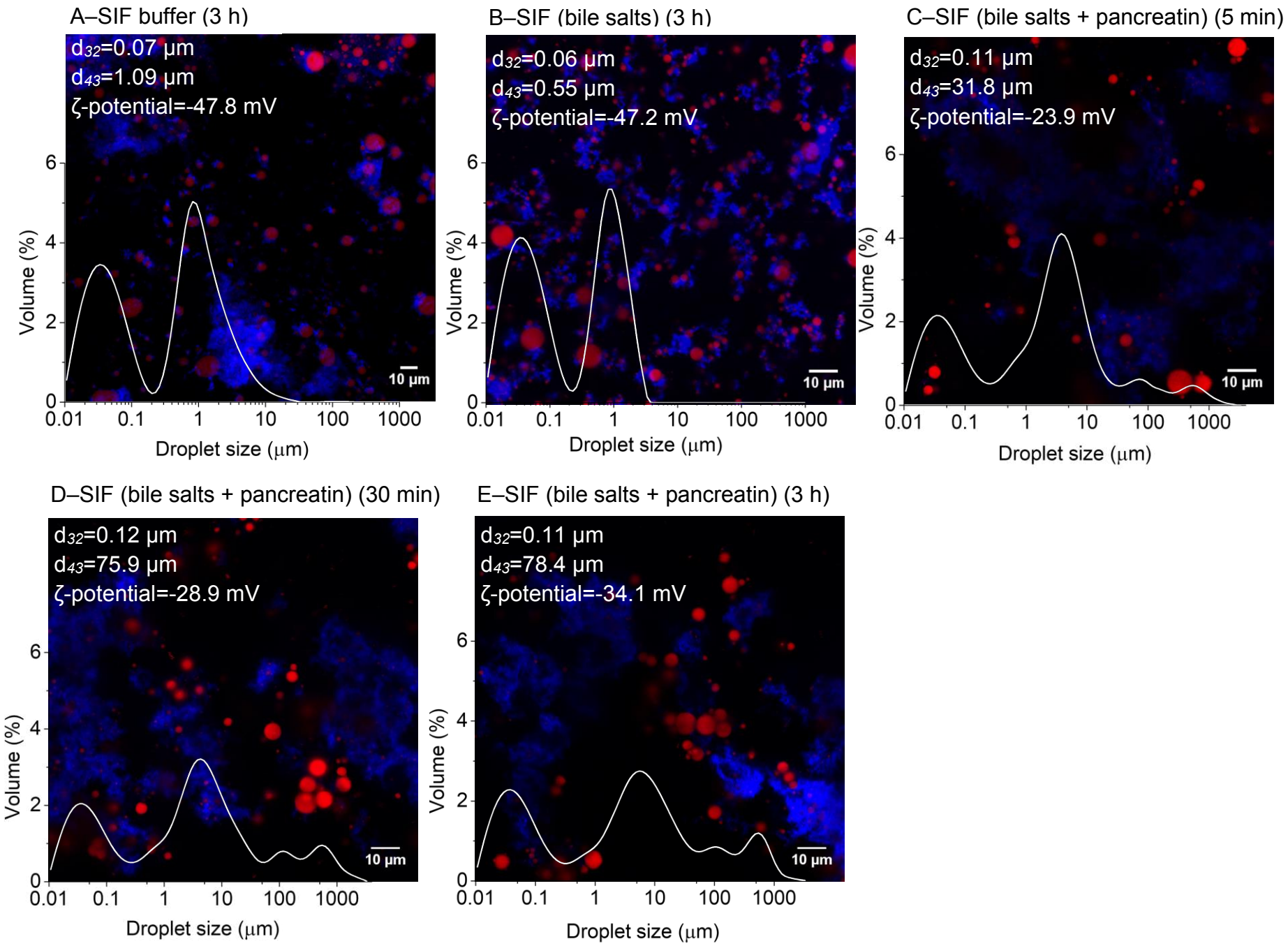
A–SIF buffer (3 h)
d32=0.07 μm
d43=1.09 μm
ζ-potential=-47.8 mV
B–SIF (bile salts) (3 h)
d32=0.06 μm
d43=0.55 μm
ζ-potential=-47.2 mV
C–SIF (bile salts + pancreatin) (5 min)
d32=0.11 μm
d43=31.8 μm
ζ-potential=-23.9 mV
D–SIF (bile salts + pancreatin) (30 min)
d32=0.12 μm
d43=75.9 μm
ζ-potential=-28.9 mV
E–SIF (bile salts + pancreatin) (3 h)
d32=0.11 μm
d43=78.4 μm
ζ-potential=-34.1 mV
10 μm
Volume (%)
Droplet size (μm)
0
2
4
6
0.01
0.1
1
10
100
1000

Figure 4

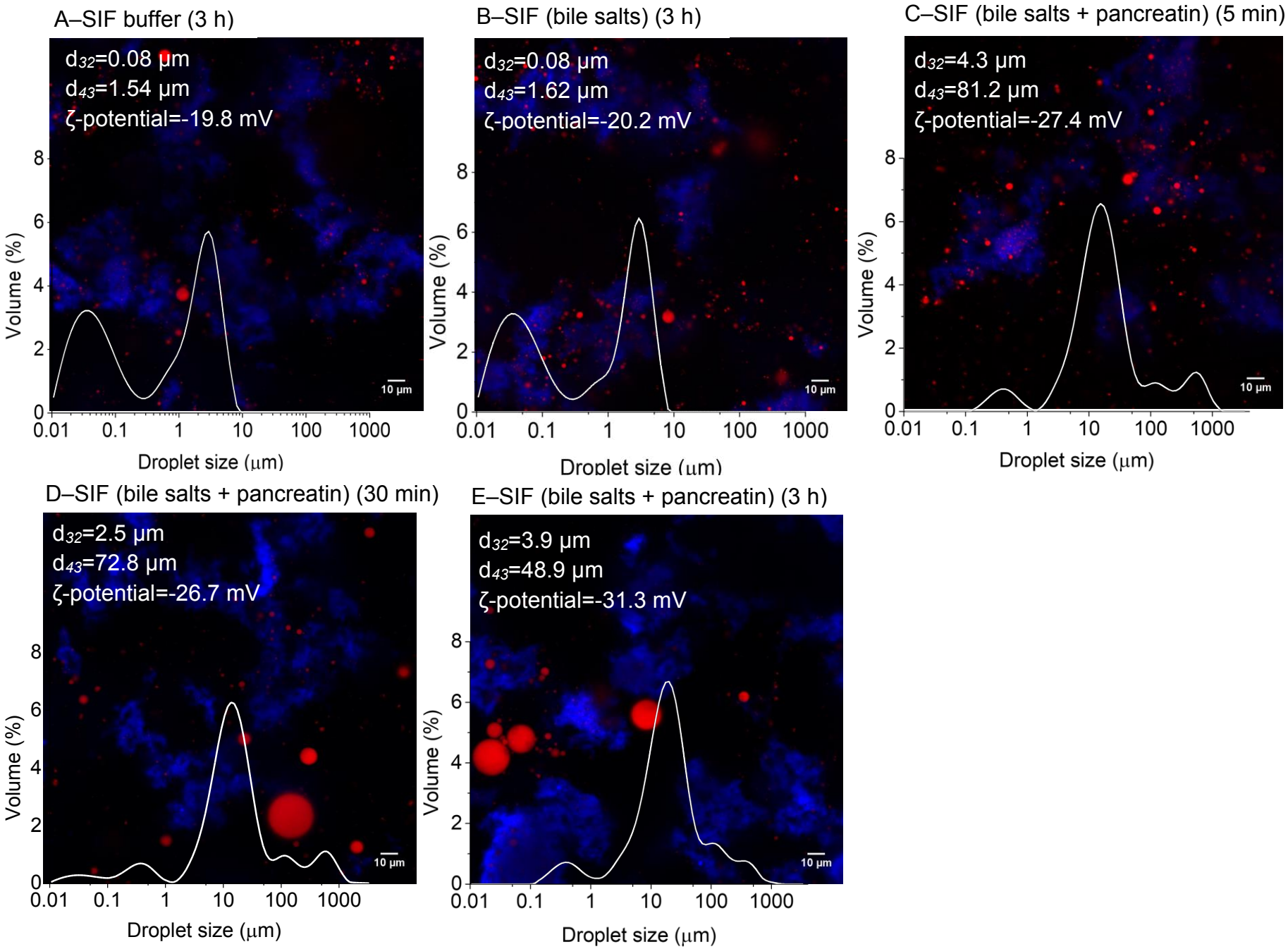
A–SIF buffer (3 h)
d32=0.08 µm
d43=1.54 µm
ζ-potential=-19.8 mV
B–SIF (bile salts) (3 h)
d32=0.08 µm
d43=1.62 µm
ζ-potential=-20.2 mV
C–SIF (bile salts + pancreatin) (5 min)
d32=4.3 µm
d43=81.2 µm
ζ-potential=-27.4 mV
D–SIF (bile salts + pancreatin) (30 min)
d32=2.5 µm
d43=72.8 µm
ζ-potential=-26.7 mV
E–SIF (bile salts + pancreatin) (3 h)
d32=3.9 µm
d43=48.9 µm
ζ-potential=-31.3 mV
10 µm
Volume (%)
Droplet size (µm)
0
2
4
6
8
0.01
0.1
1
10
100
1000

Figure 5

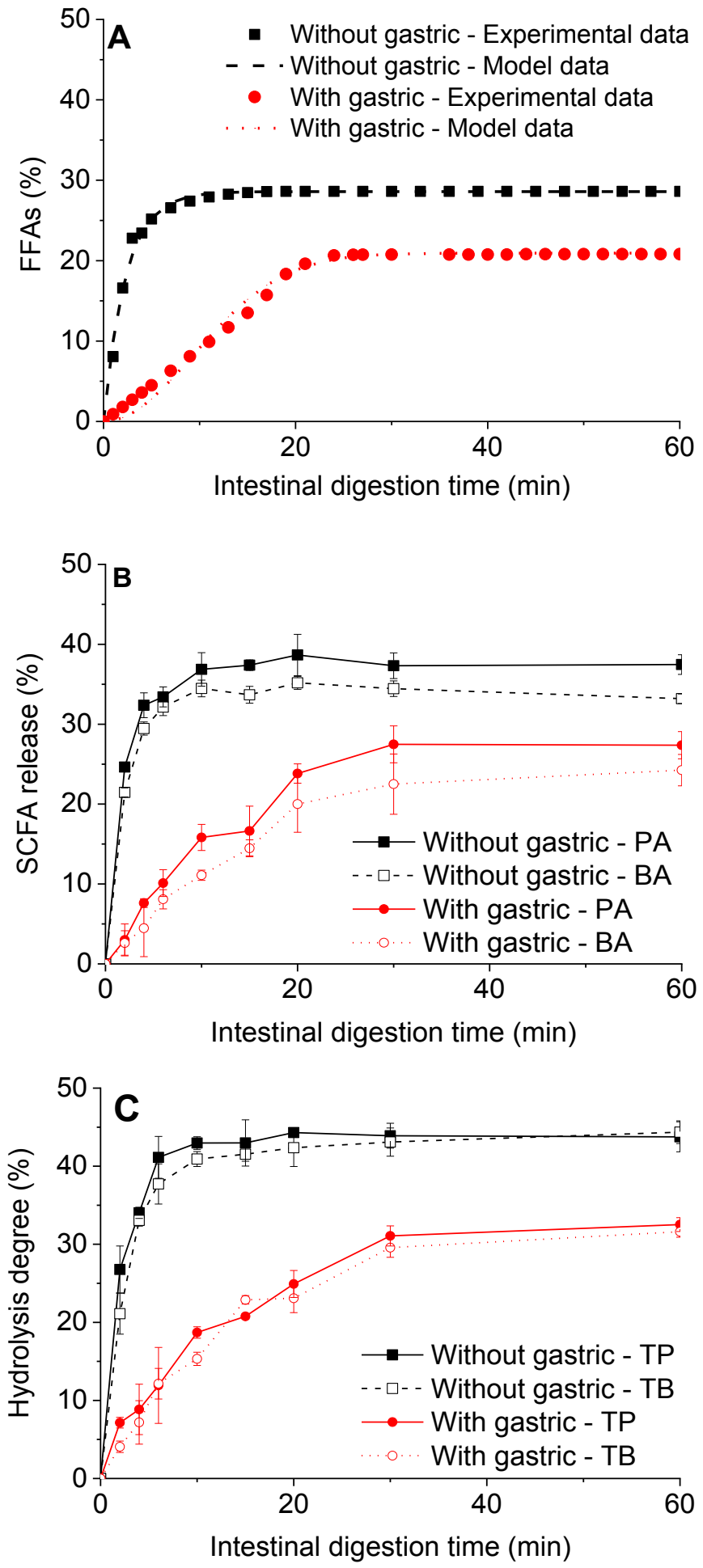
A
Without gastric - Experimental data
Without gastric - Model data
With gastric - Experimental data
With gastric - Model data
FFAs (%)
Intestinal digestion time (min)
B
SCFA release (%)
Without gastric - PA
Without gastric - BA
With gastric - PA
With gastric - BA
Intestinal digestion time (min)
C
Hydrolysis degree (%)
Without gastric - TP
Without gastric - TB
With gastric - TP
With gastric - TB
Intestinal digestion time (min)

Captions for figures

Fig. 1. Confocal images of (A) freshly prepared emulsion at pH 7.0, (B) mixture of freshly prepared emulsion and SGF buffer at pH 3.0 without the addition of pepsin and (C) mixture of freshly prepared emulsion and SGF buffer at pH 3.0 with the addition of pepsin after 2 h of incubation at 37 ^{o}C (A1, B1 and C1: MCNC channels; A2, B2 and C2: merged channels of MCNCs, pepsin and oil droplets); blue colour represents the MCNCs (stained by Calcofluor white), green colour represents the pepsin (stained by Fast green) and red colour represents the oil phase (stained by Nile red); the insets provide the corresponding droplet size distribution, d_{32} and d_{43}, values of the emulsion or digesta. The droplet volume fractions of the emulsion samples were 10 wt% because of the dilution with SGF.

Fig. 2. Mean ζ-potential values of freshly prepared emulsion (pH 3.0 and pH 7.0) and mixtures of freshly prepared emulsion and SGF buffer at pH 3.0 without and with the addition of pepsin after 2 h of incubation at 37 ^{o}C (pH 3.0). Error bars represent the standard deviations. Different superscripts (a–c) represent significant differences at the $p < 0.05$ level.

Fig. 3. Confocal images of the intestinal-digested samples at pH 7.0: (A) emulsion with SIF buffer; (B) emulsion with SIF buffer containing bile salts after 3 h of incubation at 37 ^{o}C; (C, D and E) emulsion with SIF buffer containing bile salts and pancreatin after 5 min, 30 min and 3 h of incubation at 37 ^{o}C respectively; blue colour represents the MCNCs (stained by Calcofluor white) and red colour represents the oil phase (stained by Nile red); the insets provide corresponding droplet size distribution, d_{32} and d_{43}, and ζ-potential values of the digesta. The

droplet volume fractions of the emulsion samples were 5 wt% because of the dilution with SGF and SIF.

Fig. 4. Confocal images of the sequential gastrointestinal-digested samples at pH 7.0: (A) mixture of emulsion + SGF buffer (pepsin) with SIF buffer; (B) emulsion + SGF buffer (pepsin) with SIF buffer (bile salts) after 3 h of incubation at 37 ^{o}C; (C, D and E) emulsion + SGF buffer (pepsin) with SIF buffer (bile salts and pancreatin) after 5 min, 30 min and 3 h of incubation at 37 ^{o}C respectively; blue colour represents the MCNCs (stained by Calcofluor white) and red colour represents the oil phase (stained by Nile red); the insets provide corresponding droplet size distribution, d_{32} and d_{43}, and ζ-potential values of the digesta. The droplet volume fractions of the emulsion samples were 5 wt% because of the dilution with SGF (containing pepsin) and SIF.

Fig. 5. Intestinal lipolysis profiles of the emulsions (experimental and theoretically fitted model) with or without passing through the gastric phase during in vitro digestion: (A) kinetics of total FFAs were determined by titration; (B) release of individual SCFAs (PA and BA) was quantified by GC; (C) hydrolysis proportions of TP and TB were analysed by GC. Error bars represent the standard deviations.

CRediT authorship contribution statement

Hoang Du Le: Writing - original draft, Methodology, Validation, Formal analysis, Investigation, Data curation, Writing - review & editing, Visualization, Project administration. **Simon M. Loveday**: Methodology, Supervision, Writing - review & editing. **Harjinder Singh**: Methodology, Validation, Conceptualization, Supervision, Funding acquisition, Writing - review & editing. **Anwesha Sarkar**: Methodology, Validation, Conceptualization, Data curation, Formal Analysis, Writing - review & editing, Visualization, Supervision.

Conflict of Interests

'Declarations of interest: none

Supplementary Data

Gastrointestinal digestion of Pickering emulsions stabilised by hydrophobically modified cellulose nanocrystals: release of short-chain fatty acids

Hoang Du Le[a,b], Simon M. Loveday[b,c], Harjinder Singh[b], Anwesha Sarkar[a,*]

[a] *Food Colloids and Bioprocessing Group, School of Food Science and Nutrition, University of Leeds, Leeds LS2 9JT, UK*

[b] *Riddet Institute, Massey University, Private Bag 11 222, Palmerston North 4442, New Zealand*

[c] *Food and Bio-based Products Group, AgResearch Ltd, Private Bag 11 008, Palmerston North 4442, New Zealand*

***Corresponding author:**
E-mail address: A.Sarkar@leeds.ac.uk (A.Sarkar).
Food Colloids and Bioprocessing Group,
School of Food Science and Nutrition,
University of Leeds, Leeds LS2 9JT, UK.

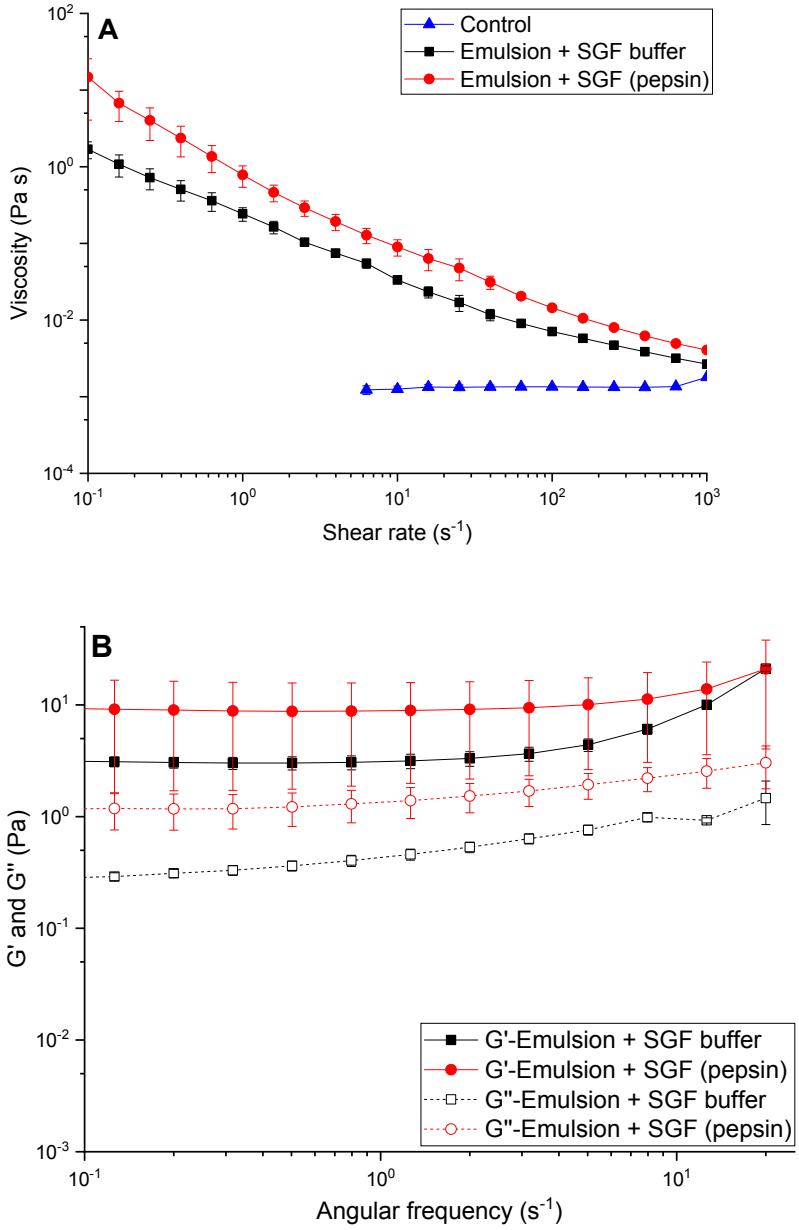

Fig. S1. (A) Apparent viscosities of control (diluted freshly prepared emulsion, i.e. 10 wt% oil) and mixtures of the freshly prepared emulsion with SGF buffer without added pepsin (Emulsion + SGF buffer) and with added pepsin [Emulsion + SGF (pepsin)] at shear rates ranging from 0 to 1000 s^{-1}. (B) Storage modulus (*G′*) and viscous modulus (*G″*) of the two systems [Emulsion + SGF buffer and Emulsion + SGF (pepsin)] at angular frequencies ranging from 0.1 to 20 s^{-1}. The plotted values are the average of at least three measurements on triplicate samples (n = 3 × 3).

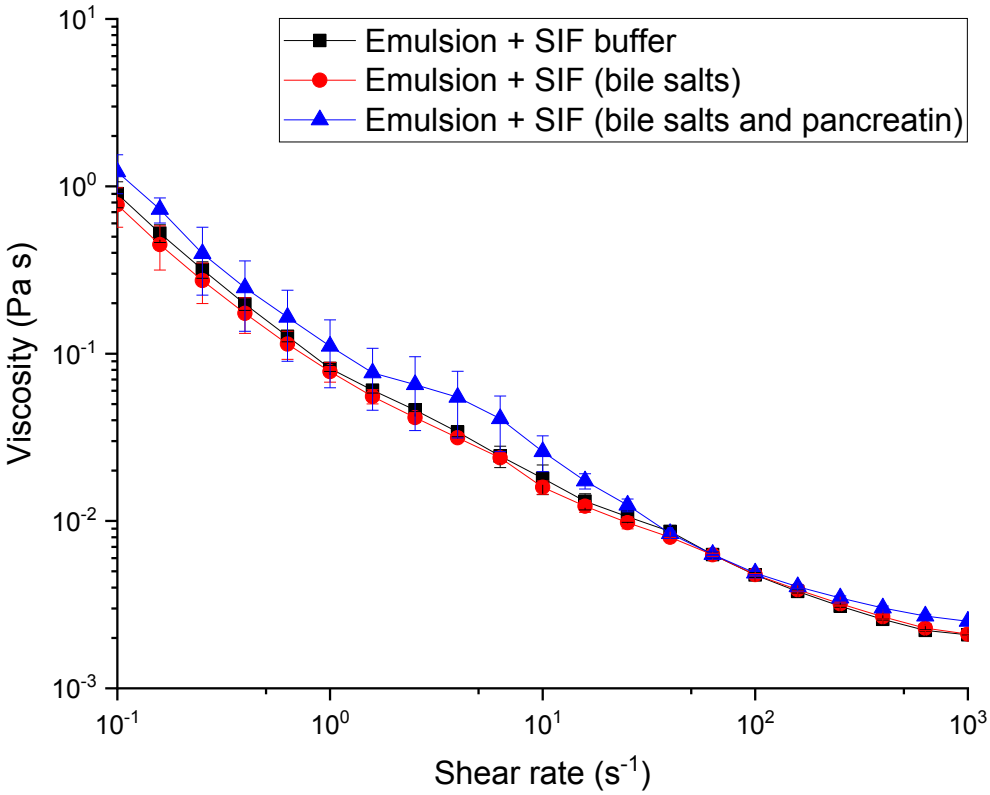

Fig. S2. Apparent viscosities of the intestinal–digested samples from freshly prepared emulsions: (1) emulsion with SIF buffer; (2) emulsion with SIF buffer containing bile salts; (3) emulsion with SIF buffer containing bile salts and pancreatin after 3 h of digestion at 37 °C at shear rates ranging from 0 to 1000 s^{-1}. The plotted values are the average of at least three measurements on triplicate samples (n = 3 × 3).

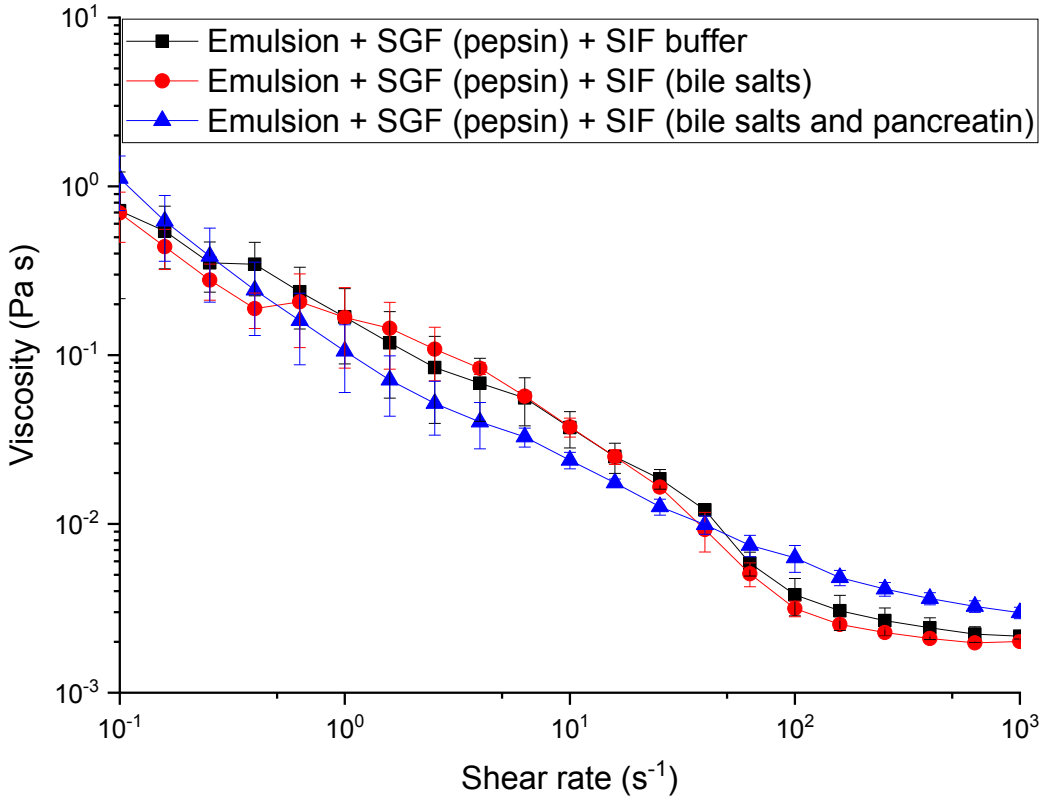

Fig. S3. Apparent viscosities of the sequential gastrointestinal-digested samples: (1) emulsion + SGF (pepsin) with SIF buffer; (2) emulsion + SGF (pepsin) with SIF buffer containing bile salts; (3) emulsion + SGF (pepsin) with SIF buffer containing bile salts and pancreatin after 3 h of digestion at 37 °C at shear rates ranging from 0 to 1000 s^{-1}. The plotted values are the average of at least three measurements on triplicate samples (n = 3 × 3).

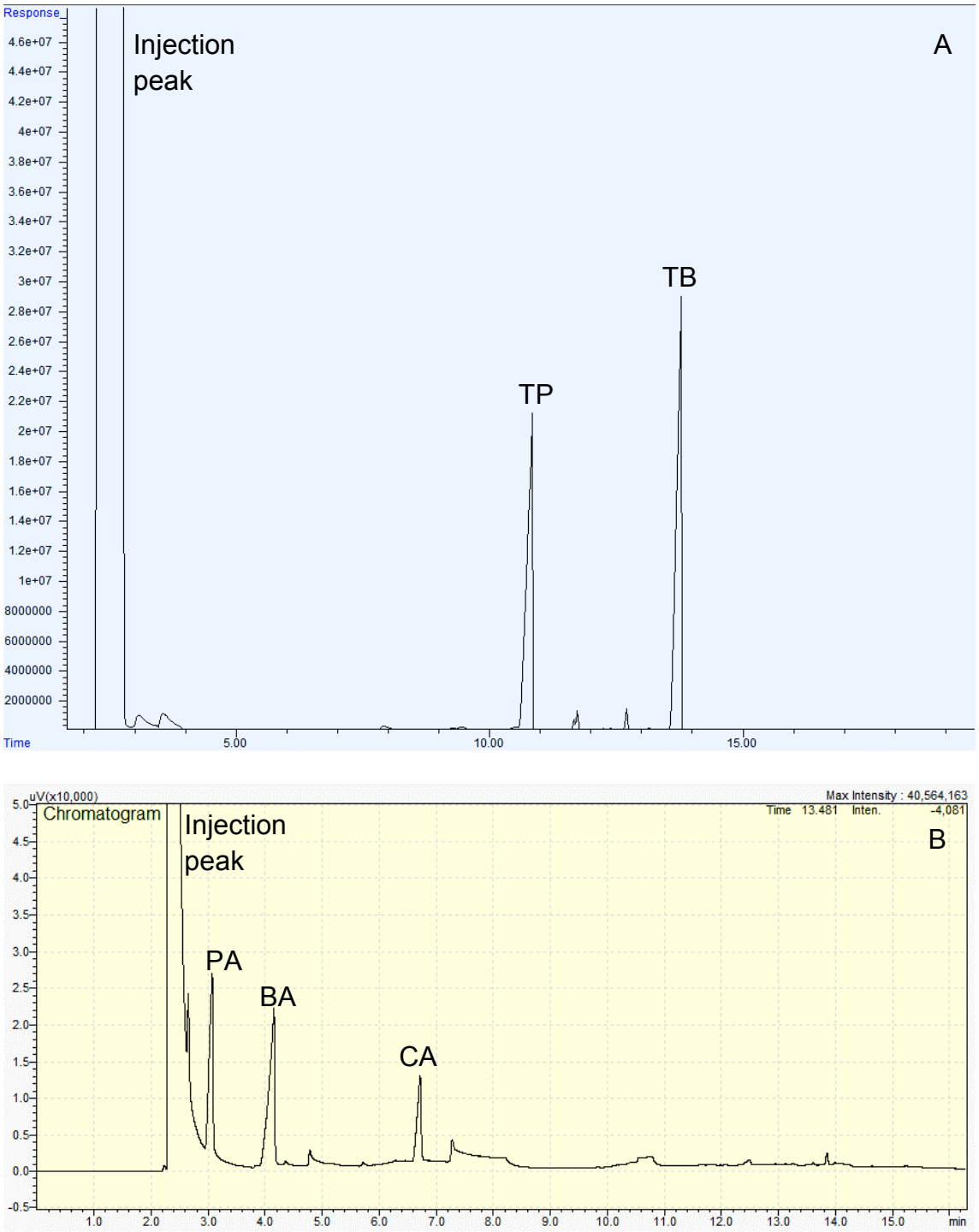

Fig. S4. GC profiles of (A) short-chain triglycerides and (B) SCFAs of the sequential gastrointestinal-digested sample after 10 min of digestion.